Hindawi Publishing Corporation
Mathematical Problems in Engineering
Volume 2015, Article ID 382483, 7 pages
http://dx.doi.org/10.1155/2015/382483

Research Article

A Wide Tuning-Range CMOS VCO with a Tunable Active Inductor

Hsuan-Ling Kao, Ping-Che Lee, and Hsien-Chin Chiu

Department of Electronic Engineering, Chang Gung University, Taoyuan City 33302, Taiwan

Correspondence should be addressed to Hsuan-Ling Kao; snoopy@mail.cgu.edu.tw

Received 9 August 2014; Accepted 26 December 2014

Academic Editor: Zhenhai Shao

This study describes a wide tuning-range VCO using tunable active inductor (TAI) topology and cross-coupled pair configuration for radio frequency operation. The TAI used two feedback loops to form a cascode circuit to obtain more degrees of freedom for inductance value. The TAI-VCO was fabricated using a 0.18 μm CMOS technology. The coarse frequency tuning is achieved by TAIs while the fine tuning is controlled by varactors. The fabricated circuit provides an output frequency range from 0.6 to 7.2 GHz (169%). The measured phase noise is from −110.38 to −86.01 dBc/Hz at a 1 MHz offset and output power is from −11.11 to −3.89 dBm within the entire frequency range under a 1.8 V power supply.

1. Introduction

The rapidly developing wireless and communication systems make the multiband RF terminals from several hundred megahertz to gigahertz frequency coexist. Integrated multiband wireless blocks in one-chip IC are demanded for high-speed, high-functionality, small-size, and low-cost communication systems. One of the key building blocks is fully integrated voltage controlled oscillators (VCOs). The challenges of the VCO circuit are die size, cost, and power dissipation. The general VCO circuits used spiral inductors and varactors to realize the circuit. However, the on-chip spiral inductors have a small inductance value per unit area and low Q-factor because of losses of Si-substrate. It also occupied a large chip size. The varactors limited the tuning range within 30% due to the maximum to the minimum capacitance ratio of the varactor and the parasitic effect [1–3]. Therefore, various techniques have been proposed to enhance the tuning range of VCOs, such as switched capacitor arrays [4–8], switched inductors [9–11], and tunable active inductors (TAIs) [12–16]. TAI is one of the good candidates due to its small size, high Q, widely tunable inductance, and large inductance compared to those of the spiral inductor [17, 18]. The tuning range of 120% (0.5~2 GHz) is achieved in a single-end VCO circuit with a TAI tuned by tunable feedback resistance [14]. A differential TAI is proposed to achieve a 0.5~3 GHz (143%) tuning range and −118 dBc/Hz at a 1 MHz offset at 690 MHz [15]. However, the operation frequencies are lower than 3 GHz because the traditional active inductor is difficult to operate at higher frequency due to a large parasitic load capacitance. The cascode active inductor (AI) is proposed to enhance the resonance frequency [17]. In this study, by utilizing a tunable cascade active inductor, the VCO circuit exhibits a very wide frequency tuning range and also enhances output power and phase noise. The TAI-VCO provides an output frequency which ranges from 0.6 to 7.2 GHz (169%). The paper is organized as follows. Section 2 outlines tunable active inductor design. Section 3 presents the TAI-VCO circuit design. Section 4 presents the TAI-VCO measurement results. Finally, concluding remarks are offered.

2. Tunable Active Inductor Design

Figure 1 shows that the proposed AI circuit consists of four transistors ($M_1 \sim M_4$) and three current sources ($I_1 \sim I_3$). Two feedback loops are formed in this circuit. Transistors M_1 and M_2 make up the first feedback loop and M_3 and M_4 form the second loop. The cascode technique is used to reduce output conductance and enhance the gain for high frequency. Transistor M_3 is stacked on top of transistor M_1. For increasing the cascode effect, the additional gain stage was implemented by M_4. The addition of transistor M_4 does

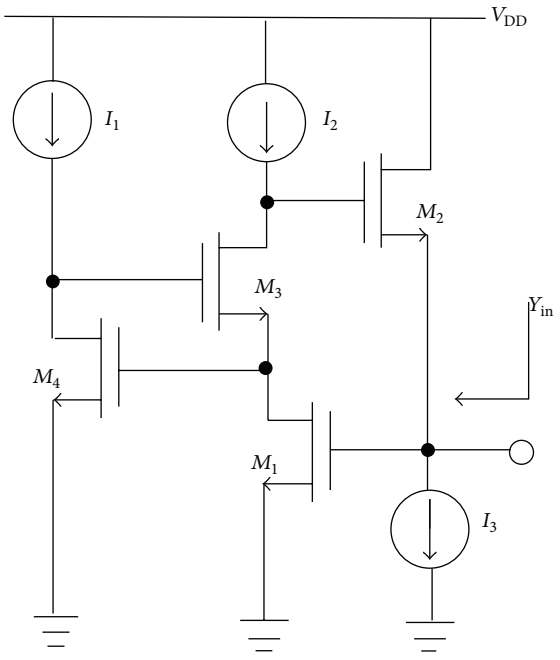

FIGURE 1: Schematic of cascode active inductor.

not degrade the high frequency response of the inductor, because the signal path is still through M_1, M_2, and M_3. To analyze the response of the TAI, the simplified small signal model and equivalent circuit model are shown in Figure 2.

The input admittance from the input port is given by the following equation:

$$Y_{in} = sC_{gs1} + \frac{g_{m1}g_{m2}}{sC_{gs2}\left(1 + s\left(C_{gs3}/g_{m3}\right) + s^2\left(C_{gs3}/g_{m3}\right)\left(C_{gs4}/g_{m4}\right)\right)} + \frac{g_{m1}}{1 + s\left(C_{gs3}/g_{m3}\right) + s^2\left(C_{gs3}/g_{m3}\right)\left(C_{gs4}/g_{m4}\right)}, \quad (1)$$

where $g_{m1} \sim g_{m4}$ are the transconductance of the transistors M_1–M_4. C_{gs} and C_{gd} are gate-source capacitance and gate-drain capacitance of the corresponding transistors, respectively. The C_{gs} is much greater than C_{gd}. The C_{gd} was ignored in the small signal model. Assume that the operating frequency (ω) of the active inductor is much lower than the cutoff frequency ($\omega_t = g_m/C_{gs}$) of the transistors. Compare (1) with the equivalent circuit in Figure 2(b) with the following values:

$$C_{eq} \approx C_{gs1} \quad (2)$$

$$G_p = \frac{1}{R_p} \approx \frac{g_{m1}}{1 - \omega^2\left(C_{gs4}C_{gs3}/g_{m3}g_{m4}\right)} = \frac{g_{m1}}{1 - \omega^2/\omega_{t3}\omega_{t4}} \quad (3)$$

$$L_{eq} \approx \frac{C_{gs2}}{g_{m1}g_{m2}}\left(1 - \frac{\omega^2 C_{gs3}C_{gs4}}{g_{m3}g_{m4}}\right) = \frac{1}{g_{m1}\omega_{t2}}\left(1 - \frac{\omega^2}{\omega_{t3}\omega_{t4}}\right) \quad (4)$$

$$R_{eq} \approx -\frac{\omega^2 C_{gs2}C_{gs3}}{g_{m1}g_{m2}g_{m3}} = -\frac{\omega^2 C_{gs2}}{g_{m1}g_{m2}\omega_{t3}} = -\frac{\omega^2}{g_{m1}\omega_{t2}\omega_{t3}}, \quad (5)$$

where $\omega_{t1} \sim \omega_{t4}$ are the transconductance of the transistors M_1–M_4. R_{eq} is very small because its value is a second-order effect. We neglect the R_{eq} in the following derivation of resonant frequency (ω_{RES}) of the active inductor which is given by

$$\omega_{RES} = \sqrt{\frac{g_{m1}g_{m2}}{C_{gs1}C_{gs2}\left(1 - \omega^2\left(C_{gs3}C_{gs4}/g_{m3}g_{m4}\right)\right)}} = \sqrt{\frac{\omega_{t1}\omega_{t2}}{\left(1 - \omega^2/\omega_{t3}\omega_{t4}\right)}}. \quad (6)$$

To evaluate the broadband characteristics of the active inductors, the quality factor (Q-factor) is defined as the ratio of the imaginary part to the real part of the input impedance, which can be approximated by

$$Q \approx \left(\omega^2\frac{C_{gs1}}{g_{m1}}\left(\frac{C_{gs2}}{g_{m2}}\right) - \omega^2\left(\frac{C_{gs2}}{g_{m2}}\right)\frac{C_{gs3}}{g_{m3}} + \omega^2\frac{C_{gs4}}{g_{m4}}\frac{C_{gs3}}{g_{m3}} - 1\right)\left(\omega\left(\frac{C_{gs2}}{g_{m2}}\right) - \omega\frac{C_{gs3}}{g_{m3}}\right)^{-1} = \frac{\omega^2/\omega_{t2}\omega_{t1} - \omega^2/\omega_{t2}\omega_{t3} + \omega^2/\omega_{t3}\omega_{t4} - 1}{\omega/\omega_{t2} - \omega/\omega_{t3}}. \quad (7)$$

From (4) and (6), it is observed that L_{eq} is inversely dependent on $g_{m1} \times \omega_{t2}$ and ω_{RES} is dependent on $(\omega_{t1}\omega_{t2})^{1/2}$. The cutoff frequency of cascode transistors ω_{t3} and ω_{t4} decreased L_{eq} and increased G_p and ω_{RES}. The small inductance and higher resonance frequency of AI provide high operation frequencies.

To achieve the tunable active inductor, M_5 is used as a current source (I_2) controlled by gate voltage (V_{ctrl}) as shown in Figure 3. The device gate width of $M_1 \sim M_5$ is 6 × 64, 3 × 40, 8 × 64, 6 × 64, and 1.5 × 25 μm, respectively. The R_1 is a current source of 156 Ω. Figure 4 shows that the g_{m1} and ω_{t2} are dependent on V_{ctrl}. The larger the V_{ctrl} is, the larger the g_{m1} and ω_{t2} are. According to (4) and (6), the inductance and resonant frequency of TAI can be tuned by V_{ctrl}. The inductance and Q-factor of TAI can be carried by controlling V_{ctrl} as the prediction of (4) and (6)-(7).

3. VCO Circuit Design

Figure 5 shows the proposed VCO where the LC-tank is composed of a TAI and a varactor (C_v) for frequency and the negative conductance ($-G_m$) is employed to compensate for the loss from the LC-tank. The symmetric components are identical. The cross-coupled pair VCO circuit is composed of M_6, M_7, C_{v1}, C_{v2}, C_1, C_2, TAI_1, and TAI_2. The device gate widths of M_6 and M_7 are 50 μm with six gate fingers. C_1 and C_2 are DC block capacitors. Figure 6 shows mechanisms of oscillator frequency tuning using TAIs and varactors [12]. The TAIs can be tuned over a wide range to provide coarse frequency tuning. The varactors provide a fine tuning range and LC-tank topology. Coarse tuning was achieved by TAIs and fine tuning was achieved by changing varactors. For coarse frequency tuning, TAI inductance is controlled by the controlled voltage (V_{ctrl}). For fine frequency tuning,

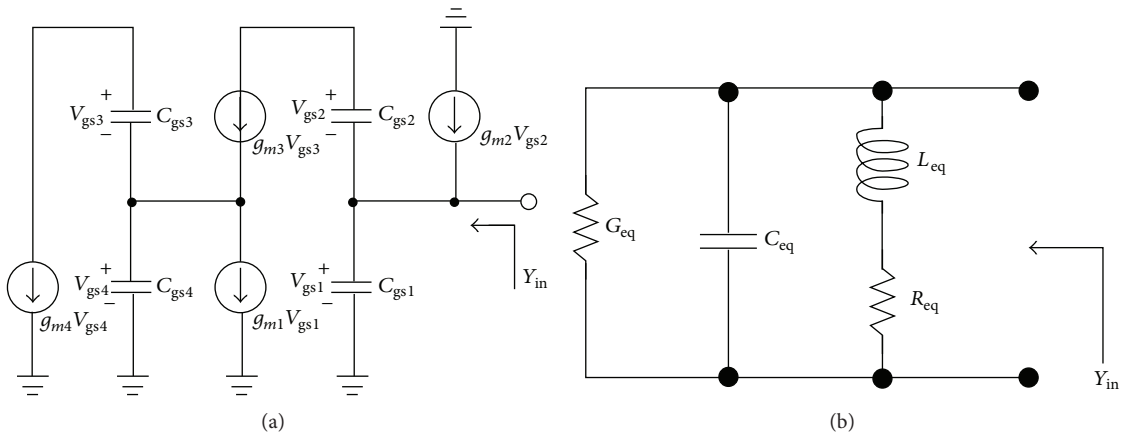

Figure 2: (a) Small-signal equivalent circuit and (b) equivalent circuit model of the AI.

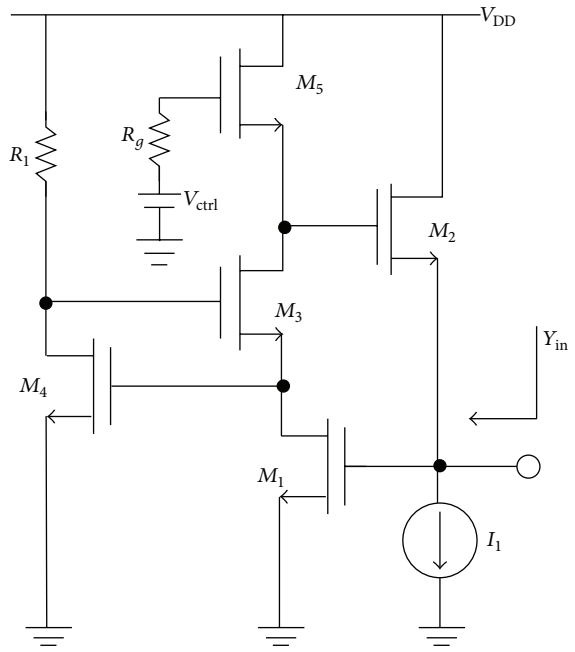

Figure 3: Tunable cascode active inductor by V_{ctrl}.

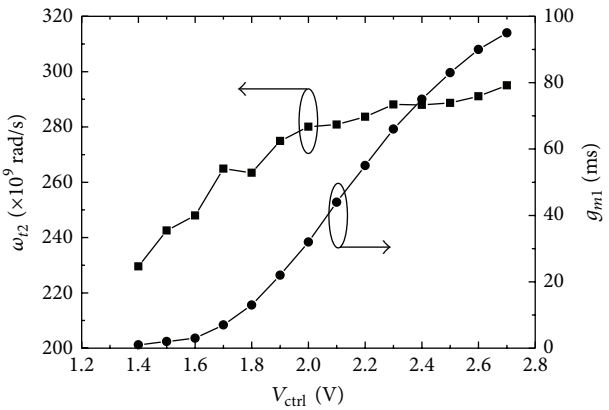

Figure 4: Simulated ω_{t2} and g_{m1} of the TAI with V_{ctrl}.

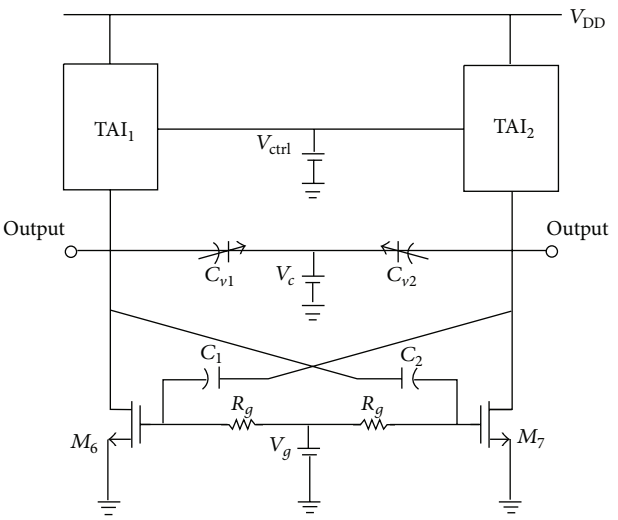

Figure 5: Schematic of the proposed TAI-VCO.

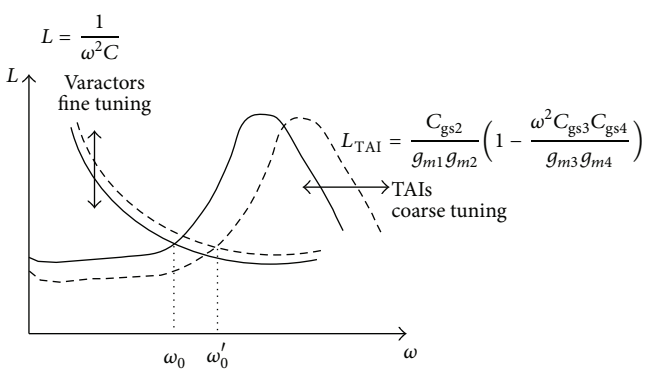

Figure 6: Mechanisms of coarse and fine tuning of the proposed TAI-VCO.

the varactor capacitance is controlled by the varactor voltage (V_c). The cross-coupled pair differential VCOs are convenient to connect directly to a differential input, such as a balanced mixer in an integrated circuit system.

The noise current injected at output nodes is composed of two parts, $\overline{i^2_{n,\mathrm{TAI}}}$ and $\overline{i^2_{n,\mathrm{CC}}}$, representing the contribution of TAI and cross-coupled pair (CC) transistors, respectively. The noise current typically is the channel-induced noise and gate-induced noise of a transistor. The total noise current of output nodes can be written as

$$\frac{\overline{i^2_{n,\mathrm{total}}}}{\Delta f} = 2\frac{\overline{i^2_{n,\mathrm{TAI}}}}{\Delta f} + \frac{\overline{i^2_{n,\mathrm{CC}}}}{\Delta f}. \tag{8}$$

The total single-sideband phase noise spectral density at an offset frequency of $\Delta\omega$ is given by

$$L\{\Delta\omega\} = 10\log\left(\frac{\sum_{n=0}^{\infty} C_n \overline{i^2_{n,\mathrm{total}}}/\Delta f}{4q^2_{\max}\Delta\omega^2}\right), \tag{9}$$

where C_n represents the coefficients in the Fourier series of the impulse sensitivity function and $q_{\max}$ is the maximum charge swing across the current noise source. The TAI and CC are composed of five and two transistors, respectively. The phase noise of TAI-VCO is larger than LC-VCO due to the number of transistors. However, the output power is also an important parameter of VCO. The coarse frequency tuning of the cascode TAI was controlled by V_{ctrl}. As V_{ctrl} increases, M_5 was driven from triode region to saturation region, resulting in larger bias current and larger drain voltage for the cross-coupled pair. Therefore, the larger drain voltage of the cross-coupled pair provided larger output swing at higher frequency while decreasing equivalent inductance and increasing oscillation frequency. A uniform output power can be achieved over the whole frequency range in the proposed TAI-VCO topology.

4. Measurement Results

The cross-coupled pair VCO was simulated, using Advance Design System (ADS) software. The layout of the circuit, especially the symmetry of the cross-coupled design, plays an important role in circuit design. The top-layer metal and bottom-layer metal crossing and the difference between path lengths are crucial to ensure balanced signals and a compact size. Figure 7 shows the layout of the fabricated VCO. Its size is $0.835 \times 0.615\ \mathrm{mm}^2$, including the probe pads. The TAI-VCO was tested on a wafer—the spectral density of the circuit being measured with a spectrum analyzer. The circuit is biased at $V_{\mathrm{DD}} = 1.8$ V, $V_g = 0.7$ V, $I_{\mathrm{total}} = 23 \sim 27$ mA, $V_{\mathrm{ctrl}} = 1.4 \sim 2.7$ V, and $V_c = 0.5 \sim 2.0$ V. The power consumption of the VCO is $41 \sim 49$ mW, from a 1.8 V power supply.

Figure 8 shows the tuning range of the TAI-VCO circuit. The proposed cross-coupled pair VCO was tuned, from 0.6 GHz to 7.2 GHz, which is a tuning range of 6.5 GHz (near 169% tuning range). Figure 9 shows the phase noise and output power of the TAI-VCO circuit. The VCO has phase noise, of −110.38 and −99.04 dBc/Hz, at a 1 MHz offset from 0.63 and 7.2 GHz carrier, respectively. Within the VCO tuning range, the variations in output power are −7.64 ± 3.5 dBm. The output spectrum and phase noise of the proposed TAI-VCO at 630 MHz, 2.7 GHz, and 7.2 GHz are shown in Figure 10. The lowest phase noise is −110.38 dBc/Hz, at 1 MHz offset from the 0.629 GHz carrier frequency. The maximum output power is −3.89 dBm, including a 4.7 dB loss due to implementation, and operates at 2.7 GHz under a 1.8 V power supply. Table 1 summarizes the measured performance

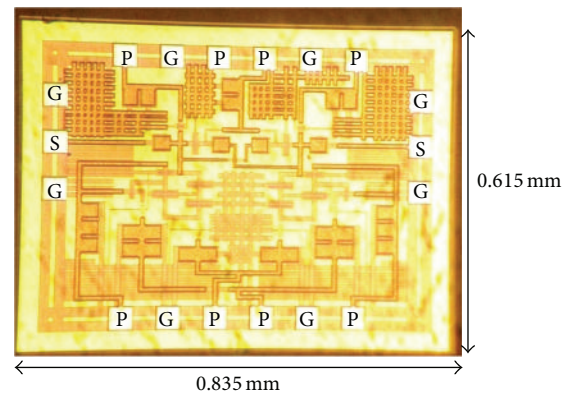

Figure 7: Photograph of the fabricated VCO.

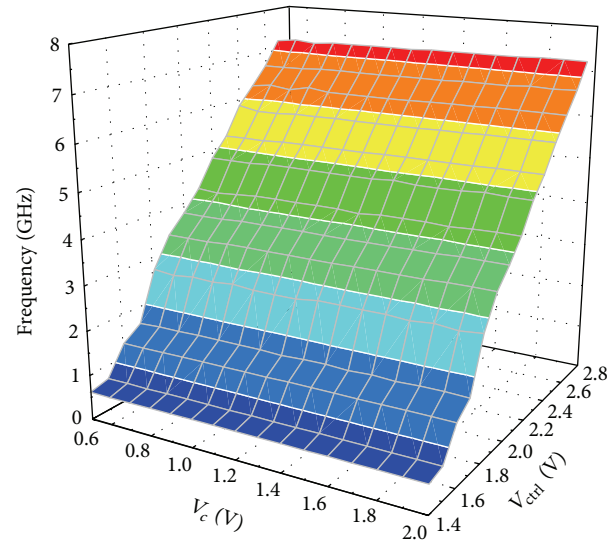

Figure 8: Measured oscillation frequency against V_{ctrl} and V_c.

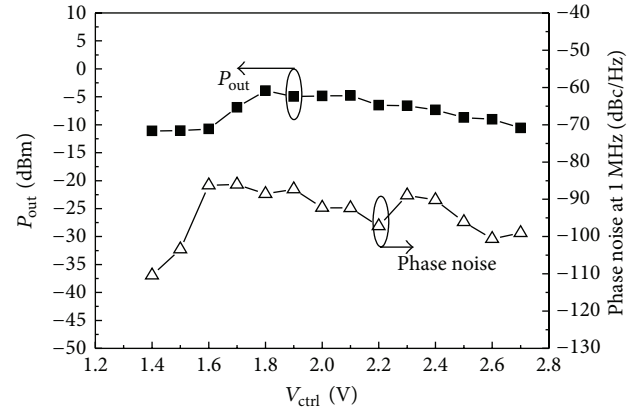

Figure 9: Measured phase noise and output power against control voltage V_{ctrl}.

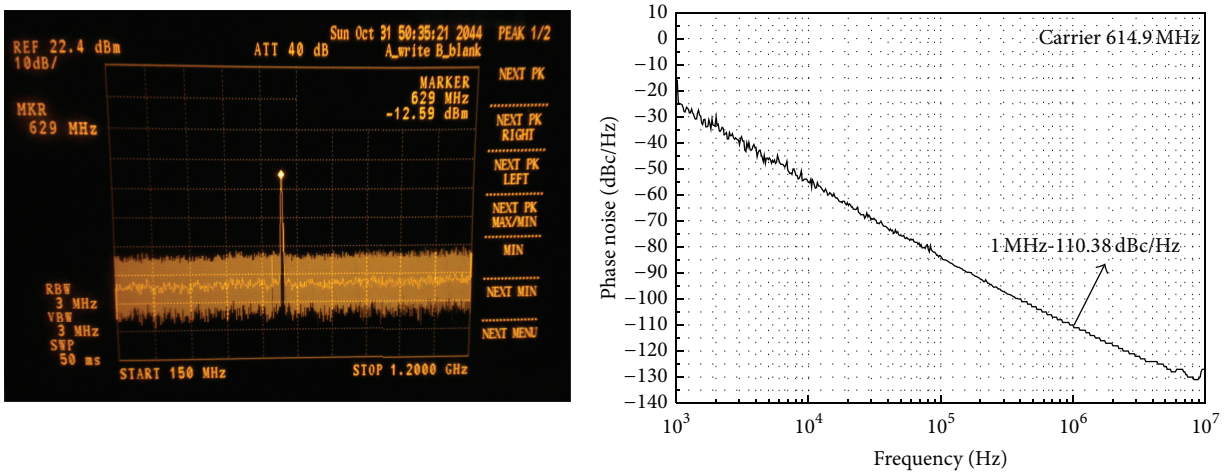

(a)

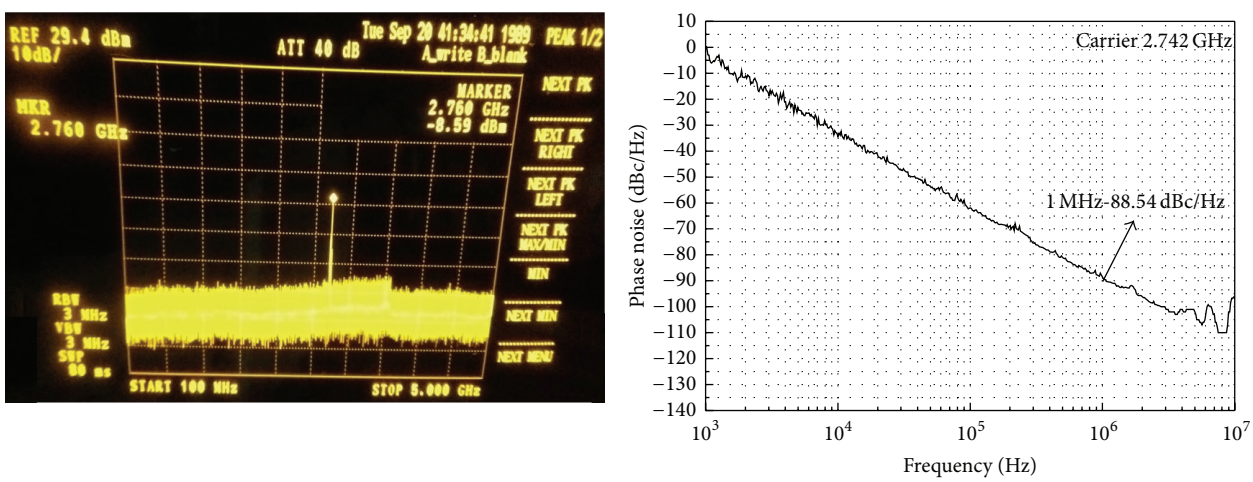

(b)

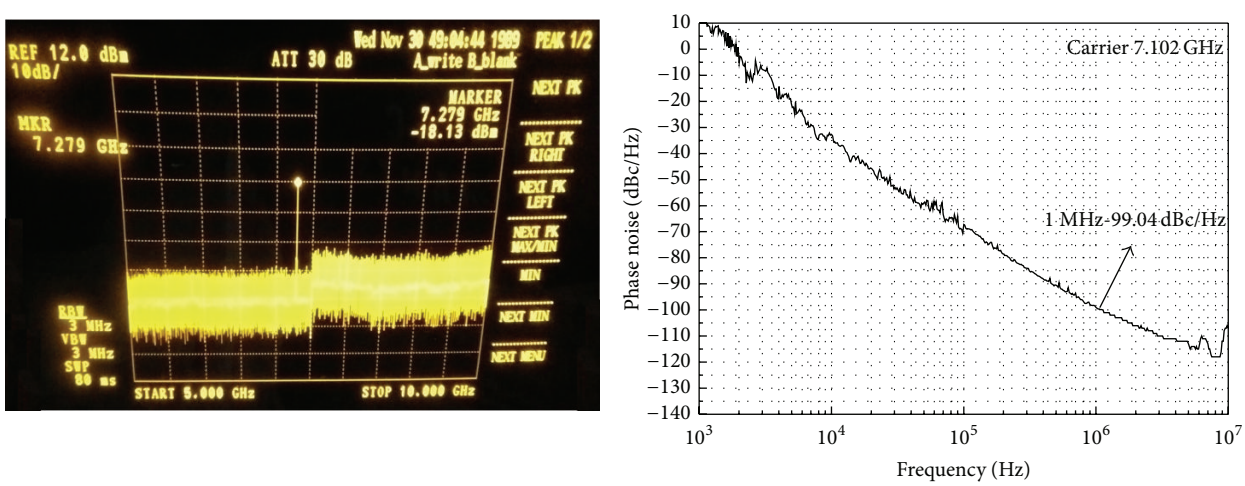

(c)

Figure 10: Output spectrum and phase noise of the proposed VCO at (a) 630 MHz, (b) 2.7 GHz, and (c) 7.2 GHz.

Table 1: Comparison of VCO circuit performance: published and this work.

	Unit	This work	[7]	[8]	[9]	[13]	[14]	[15]	[16]*
Tuning range	GHz	0.6~7.2	3.2~5.3	3.3~5.1	1.1~1.9	1.1~2.7	0.5~2	0.5~3	1.3~2.2
	%	169	47.7	41.1	51	81	120	143	47.5
KVCO	MHz/V	5,000	167~555	50~85	667	3,850	500	2,500	458
P_{out}	dBm	−3.89~−11.1	−4.8	−7	—	−14.28	−21~−29	−14~−22	−9~−16
PN at 1 MHz offset	dBc/Hz	−86~−110	−115.6	−123.14	−126	−83~−92	−78~−90	−101~−118	−82~−86
Area	mm^2	0.51	0.828	0.24	0.5	0.4	0.09	0.45	—
Architecture		TAI	Switched-cap.	Switched-cap.	Switched-ind.	TAI	TAI	TAI	TAI

*Simulated results.

of the VCO and includes other reported performances, for the purpose of comparison [7–9, 13–16].

5. Conclusion

The fully integrated VCO with tunable active inductor on 0.18 μm CMOS technology demonstrated good circuit performance, in terms of a wide tuning range, high output power, and low phase noise. This TAI-VCO displayed a wide frequency range from 0.6 to 7.2 GHz, resulting in a tuning range of 169% at radio frequency. The lowest phase noise was −110.38 dBc/Hz, at a 1 MHz offset from a 630 MHz carrier and a highest output power of −3.89 dBm at 2.7 GHz under a 1.8 V power supply.

Conflict of Interests

The authors declare that there is no conflict of interests regarding the publication of this paper.

Acknowledgments

The authors wish to thank CIC of the National Science Council and the High Speed Intelligent Communication Research Center at Chang Gung University for their help. This work was partially supported by the Ministry of Science and Technology of Taiwan (no. 103-2221-E-182 -009).

References

[1] M. Li, R. E. Amaya, R. G. Harrison, and N. G. Tarr, "Investigation of CMOS varactors for high-GHz-range applications," *Research Letters in Electronics*, vol. 2009, Article ID 535809, 4 pages, 2009.

[2] L. Jia, J. G. Ma, K. S. Yeo, X. P. Yu, M. A. Do, and W. M. Lim, "A 1.8-V 2.4/5.15-GHz dual-band LCVCO in 0.18-μm CMOS technology," *IEEE Microwave and Wireless Components Letters*, vol. 16, no. 4, pp. 194–196, 2006.

[3] B. Min and H. Jeong, "5-GHz CMOS LC VCOs with wide tuning ranges," *IEEE Microwave and Wireless Components Letters*, vol. 15, no. 5, pp. 336–338, 2005.

[4] Y. J. Moon, Y. S. Roh, C. Y. Jeong, and C. Yoo, "A 4.395.26 ghz LC-tank CMOS voltage-controlled oscillator with small VCO-gain variation," *IEEE Microwave and Wireless Components Letters*, vol. 19, no. 8, pp. 524–526, 2009.

[5] S.-L. Liu, K.-H. Chen, and A. Chin, "A dual-resonant mode 10/22-GHz VCO with a novel inductive switching approach," *IEEE Transactions on Microwave Theory and Techniques*, vol. 60, no. 7, pp. 2165–2177, 2012.

[6] Y. Ito, K. Okada, and K. Masu, "A tunable wideband frequency synthesizer using LC-VCO and mixer for reconfigurable radio transceivers," *Journal of Electrical and Computer Engineering*, vol. 2011, Article ID 361910, 7 pages, 2011.

[7] T.-P. Wang and S.-Y. Wang, "A low-voltage low-power low-phase-noise wide-tuning-range 0.18-μm CMOS VCO with high-performance FOMT of –196.3 dBc/Hz," in *Proceedings of the IEEE MTT-S International Microwave Symposium Digest (MTT '13)*, pp. 1–4, Seattle, Wash, USA, June 2013.

[8] H. Yoon, Y. Lee, J. J. Kim, and J. Choi, "A wideband dual-mode LC-VCO with a switchable gate-biased active core," *IEEE Transactions on Circuits and Systems II: Express Briefs*, vol. 61, no. 5, pp. 289–293, 2014.

[9] A. Italia, C. M. Ippolito, and G. Palmisano, "A 1-mW 1.13–1.9 GHz CMOS LC VCO using shunt-connected switched-coupled inductors," *IEEE Transactions on Circuits and Systems. I. Regular Papers*, vol. 59, no. 6, pp. 1145–1155, 2012.

[10] F. Cernoia, D. Ponton, P. Palestri et al., "Design and implementation of switched coil LC-VCOs in the GHz range using the self-inductance technique," *International Journal of Circuit Theory and Applications*, 2013.

[11] W. Zou, X. Chen, K. Dai, and X. Zou, "Switched-inductor VCO based on tapped vertical solenoid inductors," *Electronics Letters*, vol. 48, no. 9, pp. 509–511, 2012.

[12] G. Huang and B.-S. Kim, "Programmable active inductor-based wideband VCO/QVCO design," *IET Microwaves, Antennas & Propagation*, vol. 2, no. 8, pp. 830–838, 2008.

[13] Y. J. Jeong, Y. M. Kim, H. J. Chang, and T. Y. Yun, "Low-power CMOS VCO with a low-current, high-Q active inductor," *IET Microwaves, Antennas and Propagation*, vol. 6, no. 7, pp. 788–792, 2012.

[14] L.-H. Lu, H.-H. Hsieh, and Y.-T. Liao, "A wide tuning-range CMOS VCO with a differential tunable active inductor," *IEEE Transactions on Microwave Theory and Techniques*, vol. 54, no. 9, pp. 3462–3468, 2006.

[15] R. Mukhopadhyay, Y. Park, P. Sen et al., "Reconfigurable RFICs in Si-based technologies for a compact intelligent RF front-end," *IEEE Transactions on Microwave Theory and Techniques*, vol. 53, no. 1, pp. 81–93, 2005.

[16] G. Szczepkowski, G. Baldwin, and R. Farrell, "Wideband 0.18 μm CMOS VCO using active inductor with negative resistance," in *Proceedings of the European Conference on Circuit Theory and Design (ECCTD '07)*, pp. 990–993, August 2007.

[17] A. Thanachayanont and A. Payne, "VHF CMOS integrated active inductor," *Electronics Letters*, vol. 32, no. 11, pp. 999–1000, 1996.

[18] S. V. Krishnamurthy, K. El-Sankary, and E. El-Masry, "Noise-cancelling CMOS active inductor and its application in RF band-pass filter design," *International Journal of Microwave Science and Technology*, vol. 2010, Article ID 980957, 8 pages, 2010.